

**INTERCOMPARISON OF SEVEN PLANETARY LAYER/SURFACE
LAYER PHYSICS SCHEMES OVER COMPLEX TERRAIN
FOR BATTLEFIELD SITUATIONAL AWARENESS APPLICATIONS**

Richard S. Penc, Jeffrey A. Smith*, and John W. Raby,
Robert E. Dumais Jr., Brian. P. Reen, and Leelinda Dawson
US Army Research Laboratory, White Sands Missile Range, New Mexico

1 INTRODUCTION

The US Army Research Laboratory (ARL) has been performing long-term research into application of the Advanced Research version of the Weather Research and Forecast (WRF-ARW) model (Skamarock et al. 2008) for battlefield short-range forecasting in a field-deployed location. The purpose of these forecasts is to provide weather support for mission planning and execution and to augment coarser resolution models for specific applications required by field deployed units.

There are three primary goals in this research. The ultimate goal is to deploy WRF in a forward location and produce timely and useful 0- to 3-h and perhaps 0- to 6-h forecasts (nowcasts) tailored to the individual end user. Secondly, we need to increase the resolution so that user needs are met. Specifically, we require a grid spacing of roughly 1 km to resolve approximately 5-km-scale atmospheric phenomena that are necessary to resolve the detailed flow field over complex terrain.

Thirdly, there is a need to provide a measure of forecast uncertainty. Since WRE-N system operators are unlikely to have a meteorological background, the need to express forecast confidence is essential. There are a number of ways to achieve this. One is to use a time-lagged ensemble (Lu et al. 2007), which involves setting up and running the model in a rapid update cycle mode and compiling statistics and variances based on sequential model output. Another method to achieve the goal of developing a measure of uncertainty involves using physics-based ensembles (Stensrud et al. 2000). This method involves making several model runs with different physics packages selected and calculating model ensemble statistics from the model runs.

The current research has as its goal examining the performance of a number of physics packages to

see which performs best in a complex terrain environment. We selected a southern California domain that has been widely used and documented at ARL (Dumais et al. 2009, 2013; Dyer et al. 2015, 2016; Foley et al. 2015). The inner nests of this domain include coastal, transitional, mountainous, marine, urban, agricultural, forested, and desert environments. To focus on and examine the verification of surface and near-surface properties and focus on the diurnal variation of the convective boundary layer (BL) during weak synoptic forcing, we examined a number of planetary BL (PBL) options using the latest version of WRF-ARW (v.3.8.1, when this research began).

The primary goal in the current research is to determine which of the BL/SL parameterization schemes works best for generalized forward deployments where the deployed location is not known in advance. Because the modeling system is preconfigured, one scheme will be set up for use in the deployed location, regardless of location. Our modeling domain was also chosen to represent a number of geographic regions focusing on complex terrain. This goal is challenging from the standpoint of not only capturing a complex range of physical processes, land use, and elevations, but also accounting for the steep gradients in elevation, which can potentially make achieving modeling stability criteria more difficult.

2 MODEL CONFIGURATION

The numerical model used in this analysis, the WRF-ARW (Skamarock 2008), is a community weather forecast model designed and supported by NCAR. For the purposes of this study, WRF v3.8.1 was selected. This study uses a triple nest configuration of WRF-ARW centered approximately near San Diego, California (Figure 1). The domain includes a variety of geography,

* *Corresponding author address:* Jeffrey A. Smith,
US ARL, WSMR, NM, 88002, e-mail:
jeffrey.a.smith1.civ@mail.mil

land use, and topography. The marine environment, coastal environment, large valley, gently sloping desert, and mountainous terrain are all represented. Regarding land use, there are urban, suburban, agricultural, grassland, arid, and mountainous areas with a variety of subtropical and mid-latitude vegetation including grassland and forest. The domains are shown in Fig. 1. WRE-N was employed with an outer 9-km nest of 175×175 grid points (1566×1566 km) (D1), 242×241 grid points on the middle 3-km nest (720×720 km) (D2), and 127×127 grid points on the 1-km inner nest (126×126 km) (D3). The model top was selected to be 10mb. Although we concentrated on analysis of the 09-10 Feb 2012 event, additional simulations were also run for the other 4 days in our dataset. We chose to concentrate on this case since the primary intent of this study was to examine the model's ability to capture the development of the daytime CBL and transition to the nocturnal BL.

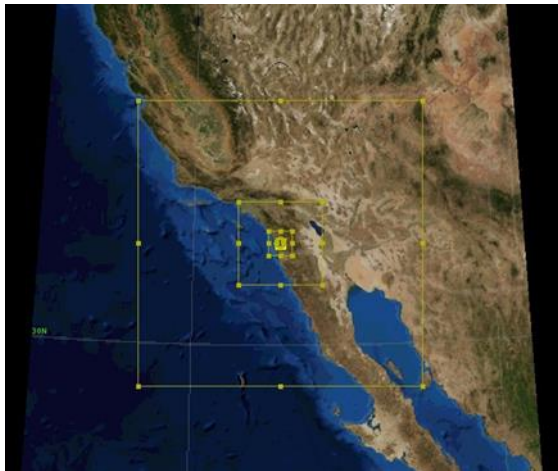


Figure 1. Location of the triple nested model domain used in these simulations.

The model specifications common to all 7 experiments using WRF-ARW as employed in this study are shown in Table 1. The FDDA option used in these model runs is based on observation nudging (Liu et al. 2005; Deng et al. 2009). This option is much less computationally expensive than traditional 4-D variational data assimilation (Huang et al. 2009) or ensemble Kalman filtering (Zupanski et al. 2008). Table 2 lists some of the data assimilated into the first 6h of the 24h forecast.

Table 1: Common configuration used in the WRF simulations for this study.

Namelist Parameter	Option Selected
Shortwave Radiation	Dudhia Scheme
Longwave Radiation	RRTM
Explicit moist microphysics	Thompson
Cumulus parameterization	Kain-Fritsch 9km only, explicit 1, 3km
PBL scheme	Varies (elsewhere)
Surface layer	Paired with PBL scheme
Land Surface Scheme	NOAH
Time step to grid ratio (s/km)	3:1
Horizontal subgrid diffusion	Second-order on coordinate surfaces
Subgrid turbulence closure	Horizontal Smagorinsky first order

Table 2: Selected data assimilation switches as configured for this study.

setting name	setting value
use_tamdar	yes
use_madis_mesonet	yes
use_madis_profiler_npn	yes
use_madis_acars	yes
use_madis_maritime	yes
use_madis_metar	yes
use_madis_raob	yes
use_madis_sao	yes
use_madis_satwin	no
use_madis_satwind1h	no
geog_data_res	2m, 30s, 30s

The 7 PBL/SL parameterization combinations selected for this study are listed in Table 3. In each of these, the default SL scheme was coupled with the PBL scheme being tested because they are generally accepted and the most widely used by researchers. Where there was a matching SL, we used that option. For the others, where multiple options existed for SL choice, we used the revised MM5 SL scheme. That scheme is reported to work with many of the PBL options.

Table 3: PBL/SL combinations evaluated.

Case no.	PBL/SL option	PBL scheme	SL scheme
1	5 / 5	Mellor-Yamada Nakanishi and Niino (MYNN)	Nakanishi and Niino PBL's SL scheme
2	11 / 1	Shin-Hong Scheme (SH)	Revised MM5 SL scheme
3	2 / 2	Mellor-Yamada-Janjic Scheme (MYJ)	Eta similarity SL scheme
4	1 / 1	Yonsei University Scheme (YSU)	Revised MM5 SL scheme
5	8 / 1	Bougeault-Lacarrère PBL (BouLac)	Revised MM5 SL scheme
6	4 / 4	Quasi-Normal Scale Elimination (QNSE)	QNSE PBL scheme's SL option
7	7 / 1	Asymmetric Convective Model (ACM2)	Revised MM5 SL scheme

3 RESULTS

Model bias and RMSE were calculated for each of the 7 members in the ensemble for each hour of the simulation, including the data assimilation (hours 1–6), the nowcast period (hours 7–12), and the extended forecast (hours 13–24). Over the model domain, these periods roughly correspond to morning, afternoon, and nighttime hours, respectively. This corresponds to, respectively, 1300 UTC 09 February 2012 through 1800 UTC 09 February (0500–1000 Pacific Standard Time [PST]), 1900 UTC 09 February 2012 through 0000 UTC 10 February 2012 (1100–1600 PST), and 0100 UTC 10 February 2012 through 1200 UTC 10 February 2012 (1700–0400 PST). In addition, the overall model statistics were computed (hours 1–24) and reflect the period 1300 UTC 09 February 2012 through 1200 UTC 10 February 2012.

All of the analyses we present apply to the innermost D3 (1-km) domain. The temperature bias is shown in Fig. 2. During the data assimilation period (1200–1800 UTC) all of the schemes show a small forecast bias, typically less than 1 K. While the ACM2, BouLac, MYJ, SH, and YSU schemes perform very similarly, the MYNN and QNSE schemes diverge, showing a negative bias, underestimating the surface temperature. The former schemes slightly overestimate the surface temperature at 2m for the hours 1400

through 1600 UTC. After hour 4 of the simulation, all of the schemes converge and tend toward underestimating the surface temperature.

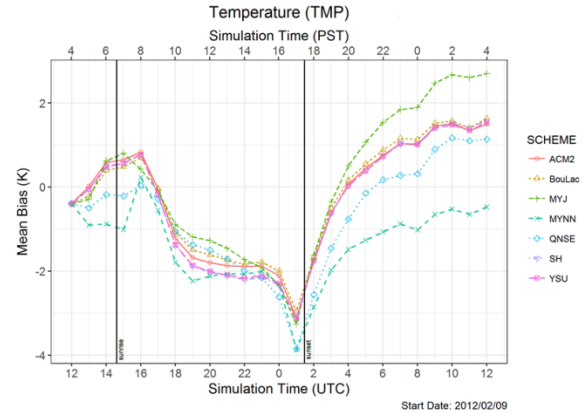


Figure 2: Temperature mean bias for the 7 members.

The bias for the DPT is shown in Fig. 3. For the majority of the forecast cycle, the DPT (at the surface) is underestimated by the model as shown by the negative bias, with the exception being between 0000 and 0200 UTC (1600–1800 PST). During these 3 h, which occur in late afternoon leading into early evening, the DPT is overestimated. Throughout the simulation, there is larger spread among the individual schemes than for the temperature bias.

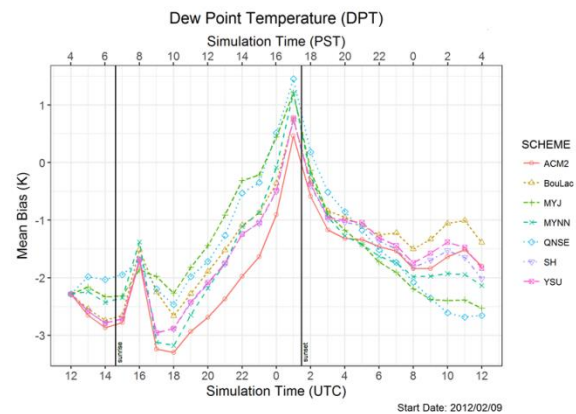


Figure 3: Dew point mean bias for the 7 members.

Looking at the surface wind speed (Fig. 4) bias we again see differing behavior for the 3 periods: assimilation, nowcast, and extended forecast. The model overestimates the surface wind during data assimilation by as much as 2 ms^{-1} but then quickly settles down to near zero

bias by 4 h into the simulation. There is more spread in the model bias by the nowcast period, with the greatest bias occurring with the QNSE scheme. QNSE overestimates the wind speed by $>1 \text{ ms}^{-1}$ from hours 9–10 of the simulation. In contrast, the ACM2 scheme underestimates the wind by as much as 1 ms^{-1} around 8 h into the simulation. As in all of the previous analyses, the model bias contrast between the 7 schemes is most pronounced for the latter half of the simulation time. For wind speed bias, the best performers at nighttime are YSU, SH, and ACM2, with near zero bias for the extended forecast period. The worst performer for the extended forecast is QNSE, followed by MYJ, with a mean bias error of approximately 1 ms^{-1} , overestimating the surface wind. Note that the physics differences appear to be most pronounced during nighttime.

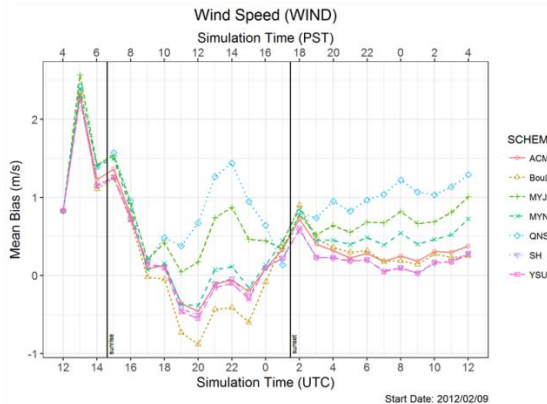


Figure 4: Wind speed mean bias for the 7 members.

We also performed an analysis of the model RMSE. The surface (2m) temperature RMSE for each of the members is shown in Fig. 5. The RMSE averages approximately 2.6 K at the beginning of the simulation time. The MYNN scheme shows the largest RMSE for the initial 4 h while QNSE shows the lowest. After 1400 UTC, the RMSE decreases to around 2 K for all of the members. For the nowcast period (6–12 h simulation time), the RMSE increases fairly linearly from about 1.5 to 3.5 K, with the highest RMSE associated with the MYNN and QNSE schemes. After 15 h, the RMSE of the members typically varies from 2.5 to 3.5 K. BouLac, ACM2, SH, and YSU follow each other closely toward the ending hours of the simulation in the extended forecast. Since SH is based on YSU, the similarity between these 2 schemes is not unexpected. The

closeness of these schemes reflects the similarity in the formulation of the physics for the nighttime case, and these times reflect the nighttime scenario over the model domain. The increase of RMSE toward the end of the simulation is not unexpected since the errors tend to be cumulative.

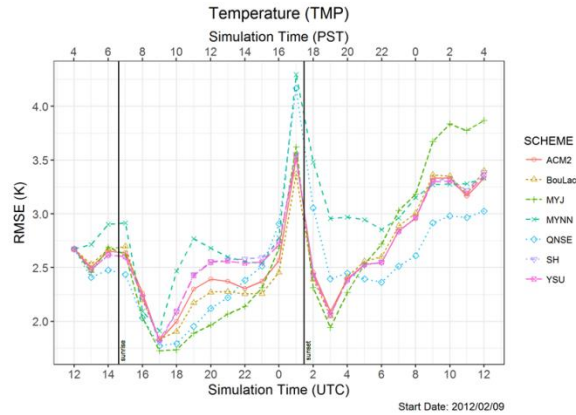


Figure 5: Temperature RMSE for the 7 members

Figure 6 shows the DPT RMSE for each of the schemes tested. The mean RMSE at the point of initialization is approximately 3.3 K, which is significant. As data assimilation progresses, the RMSE increases to approximately 3.8 K, with an increased spread among the schemes tested. During the nowcast period the RMSE decreases from approximately 4.0 to 2.5 K, corresponding to the development of the daytime CBL, and decreasing by late afternoon (1600–1800 PST). There is little spread among the model members. The most notable spread among the model members occurs during the early part of the nowcast period. MYJ, QNSE, and BouLac perform the best during this time with the lowest RMSE of all the members. MYNN and ACM2 have the highest RMSE of the 7 members during the period extending from the end of data assimilation through the early part of the 6-h nowcast period. There is overall no clearly superior scheme to choose from.

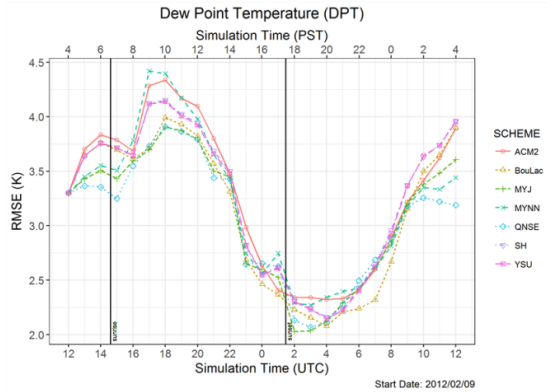


Figure 6: Dew point RMSE for the 7 members.

The wind speed RMSE for the 7 schemes is shown in Fig. 7. At model initialization, the RMSE is 1.6 ms^{-1} . RMSE then increases to over 3 ms^{-1} in the first simulation hour, then settles to about 2.5 ms^{-1} the next hour. The RMSE continues to decrease for the next 5 h to around 1.5 ms^{-1} where it remains for the remainder of the model simulation time. There is little difference between the individual schemes during the first 5 h. After that, the spread between individual BL schemes increases. During the nowcast period, which corresponds to daytime, the QNSE scheme shows the greatest RMSE, followed by BouLac and MYJ. The remaining schemes (YSU, SH, YSU, and MYNN) have the lowest RMSE. The latter half of the simulation time, during the formation and maintenance of the nighttime BL, shows the greatest spread. MYJ, SH, BouLac, and ACM2, show the least RMSE, ranging from 1.2 to 1.5 ms^{-1} . The greatest variation between schemes occurs during the nighttime. This is consistent with the analyses of temperature and RH errors presented earlier. Differences between the various BL/SL formulations appear to be greater at nighttime rather than daytime.

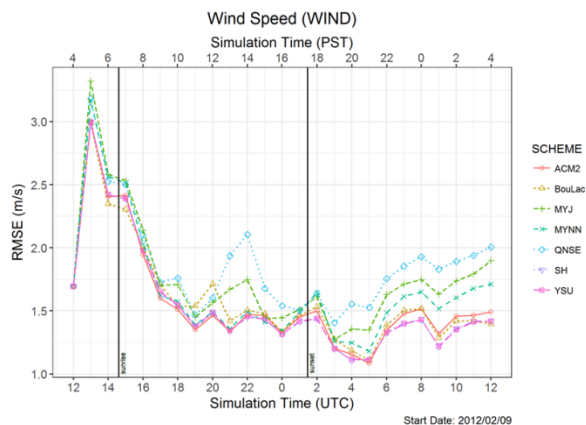


Fig. 7: Wind speed RMSE for the 7 members.

To choose the best overall scheme, we assigned rankings (from 1 through 7) for each of the 3 independent variables (T, DPT, and wind) and averaged the RMSE rankings for the nowcast, extended forecast, and complete forecast periods, for temperature, dew point, and wind speed. Since the bias calculation potentially includes large swings in the error that may be offset by one in the other direction, we evaluated the performance of the schemes using only the RMSE.

The results are shown in Table 4. We included rankings for T, DPT, and wind speed. For the nowcast period (daytime), the BouLac scheme performs best. For the extended forecast (nighttime) YSU, BouLac, and QNSE tied for best performance. Overall, for the entire forecast period, BouLac performs best for our data. The ensemble mean RMSE for temperature varies between 2.4 and 3.0 K, DPT RMSE ranges from 2.8 to 3.4 K and for wind velocity is nearly constant at approximately 1.5 ms^{-1} . The standard deviation of the RMSE is quite small, and is indicative the small differences between the various PBL schemes we tested.

4 SUMMARY AND CONCLUSIONS

We tested 7 PBL/SL parameterization schemes using a 9-/3-/1-km triple nest grid configuration centered over San Diego, California, under quiescent conditions in late winter. There was little spread in the RMSE/bias statistics for the schemes we tested. The WRF model had its greatest difficulty in capturing the transition between daytime and nighttime boundary layers for our test day. The greatest variation between schemes is with the nocturnal BL. For the nowcast period, the best overall performer was BouLac, followed by MYJ. For the extended forecast period, the YSU, BouLac, and QNSE schemes were tied for best performance. For the overall forecast period (nowcast, extended) BouLac was best, followed by QNSE. The standard deviation of the ensemble created using the various PBL schemes was small despite the fact that the schemes we tested were devised using local, nonlocal, and hybrid approaches.

While the SH scheme was developed primarily to address the scale awareness problem (Shin and Hong, 2013), we did not see an improvement in using this scheme with a 1-km grid spacing, in particular with the YSU scheme, which shares common lineage.

Independent statistical analysis by Smith et al. (2018) is in agreement with our determination of

the lack of variance between the schemes, and attributes only 3%–4% of total model variance to the PBL schemes. That calculation involves, at the highest level, an extension of a common data analytics approach called ANOVA (for analysis of variance), which uses a parameter eta (η). Bakeman (2005) found that a generalized eta squared, η_G , was superior. Eta squared (η_G^2) was calculated using the *lsr* package in R (Navarro 2015), allowing us to estimate the relative contribution to model error (uncertainty) due to the BL physics packages.

Talagrand (Hamill, 2000) diagrams were also constructed and show very little dispersion

between the 7 members. Because we did not obtain an optimal flat response in our Talagrand plots, but rather a classic “U shaped” distribution characteristic of inadequate spread between the ensemble members for all but temperature, the use of only a physics-based ensemble (in this case BL/SL combinations) is inadequate for deriving probabilistic information and forecast uncertainty. Research looking into the relative contributions to model uncertainty due to the other physics schemes and initialization data is addressed in the DoE approach described by Smith et al. (2018).

Table 4: Ranking for RMSE statistics by scheme (1=best, 7=worst)

Hours	Field	MEAN	STDEV	MYNN	SH	MYJ	YSU	BouLac	QNSE	ACM2
06 through 12 (nowcast)	Temp	2.43	0.18	7	6	1	5	2	3	4
	DPT	3.38	0.09	5	5	3	4	1	1	7
	WIND	1.49	0.12	4	1	6	1	5	7	1
	COMP			7	5	3	2	1	4	5
12 through 24 (extended)	Temp	2.95	0.15	7	3	6	2	3	1	3
	DPT	2.77	0.07	4	7	2	6	2	1	5
	WIND	1.47	0.16	5	1	6	1	4	7	3
	COMP			7	5	6	1	1	1	4
06 through 24 (complete)	Temp	2.77	0.13	7	6	4	4	2	1	3
	DPT	2.97	0.07	4	6	3	5	2	1	6
	WIND	1.47	0.14	5	1	6	1	4	7	3
	COMP			7	5	6	3	1	2	4

REFERENCES

Bakeman R. Recommended effect size statistics for repeated measures designs. *Behavior Research Methods*. 2005;37(3):379–384.

Deng A, Stauffer D, Gaudet B, Dudhia J, Bruyere C, Wu W, Vandenberghe F, Liu Y, Bourgeois A. Update on WRF-ARW end-to-end multi-scale FDDA system. *Proceedings of 10th National Center for Atmospheric Research (NCAR) WRF Users’ Workshop*. 2009 June 23–26; Boulder, CO. p. 14. .

Dumais R, Kirby S, Flanigan R. Implementation of the WRF 4-dimensional data assimilation method of observation nudging for use as an ARL weather running estimate-nowcast. Aberdeen Proving

Ground (MD): Army Research Laboratory (US); 2013 June. Report No.: ARL-TR-6485. p. 24.

Dumais R, Passner J, Flanigan R, Sauter B, Kirby S. High resolution WRF-ARW studies at the US Army Research Laboratory for use in short-range forecast operations. Short range forecast applications: P2.4. *Proceedings of the 23rd Conference on Weather Analysis and Forecasting/19th Conference on NWP*; 2009 June 1–5; Omaha, NE.

Dyer J, Zarzar C. US Army Research Laboratory (ARL)/Mississippi State University (MSU) project: atmospheric modeling and decision aids: field-based numerical weather simulations and analysis support tools period of performance: WRF on a

laptop-user's guides. White Sands (NM): Battlefield Environment Division, Army Research Laboratory (US); 2015 Sep 29. p. 31.

Dyer J, Zarzar C, Dumais R, Raby J, Smith JA. Defining the influence of horizontal grid spacing on ensemble uncertainty within a regional modeling framework. *Wea Forecast*. 2016;31:1997–2017.

Foley T, Smith J, Raby J, Reen B, Penc R. Developing sub-domain verification methods using GIS tools. Presented at the Esri User Conference; 2015 July 21; San Diego, CA.

Hamill TM. Interpretation of rank histograms for verifying ensemble forecasts. *Mon Wea Rev*. 2000;129:550–560.

Huang X, Xiao Q, Barker D, Zhang X, Michalakes J, Huang W, Henderson T, Bray J, Chen Y, Ma Z, et al. Four-dimensional variational data assimilation for WRF: formulation and preliminary results. *Mon Wea Rev*. 2009;137:299–314.

Liu Y, Bourgeois A, Warner T, Swerdlin S, Hacker J. Implementation of observation nudging based FDDA into WRF for supporting ATEC test operations. 6th National Center for Atmospheric Research (NCAR) WRF/15th MM5 Users' Workshop; 2005; Boulder, CO.

Lu C, Yuan H, Schwartz B, Benjamin S. Short-range numerical weather prediction using time-lagged ensembles. *Wea Forecast*. 2007;22:580–595.

Navarro DJ. Learning statistics with R: a tutorial for psychology students and other beginners. Version 0.5.: University of Adelaide; 2015.

Penc, R. S., J. A. Smith, J. W. Raby, R. E. Dumais, Jr., B. P. Reen, and L. P. Dawson, 2018b: Intercomparison of 7 Planetary Boundary-Layer/Surface-Layer Physics Schemes over Complex Terrain for Battlefield Situational Awareness. Technical Report ARL-TR-8353.

Skamarock W, Klemp J, Dudhia J, Gill D, Barker D, Duda M, Huang X, Wang W, Powers J. A description of the advanced research WRF Version 3. Boulder (CO): National Center for Atmospheric Research (NCAR); 2008 June. Report No.: TN-475+STR.

Smith JA, Penc RS, Raby JW. Statistical design of experiments in numerical weather prediction: emerging results. Presented at the 98th Annual American Meteorological Society Meeting/25th Conference on Probability and Statistics; 2018 Jan 7–11; Austin, TX. Paper No.: 6.1.

Stensrud DJ. Parameterization schemes: keys to understanding numerical weather prediction models. New York (NY): Cambridge University Press; 2007.

Shin H, Hong S. Analysis of resolved and parameterized vertical transports in convective boundary layers at gray-zone resolutions. *J Atmos Sci*. 2013;70:3248–3261.